Applied Catalysis B: Environmental 97 (2010) 72–81

Contents lists available at ScienceDirect

Applied Catalysis B: Environmental

journal homepage: www.elsevier.com/locate/apcatb

Preparation and characterization of bimetallic Rh-Ni/Y_2O_3-Al_2O_3 for hydrogen production by raw bioethanol steam reforming: influence of the addition of nickel on the catalyst performances and stability

Anthony Le Valant, Nicolas Bion, Fabien Can*, Daniel Duprez, Florence Epron

Laboratoire de Catalyse en Chimie organique - UMR 6503–CNRS/University of Poitiers, 40 Av. Recteur Pineau, F-86022 Poitiers Cedex, France

ARTICLE INFO

Article history:
Received 22 January 2010
Received in revised form 19 March 2010
Accepted 19 March 2010
Available online 27 March 2010

Keywords:
Rhodium
Nickel
Ethanol steam reforming
Rare earth elements
Yttrium
Hydrogen production
Impurity
Methyl-2-propan-1-ol
Infrared study
Bimetallic catalysts

ABSTRACT

The influence of the addition of Ni on the catalytic behaviour of a Rh/Y_2O_3-Al_2O_3 catalyst (Rh/Y-Al) was evaluated in the ethanol steam reforming reaction in the presence of methyl-2-propan-1-ol as impurity. Physical-chemical properties of modified materials were determined by H_2 chemisorption, XRD, BET, TPR, IR spectroscopy and TPO. It was established that the catalytic behaviour of the Rh/Y-Al base catalyst is widely improved by the addition of Ni. Nickel incorporation leads to the formation of both dispersed nickel phase and nickel aluminate species. Basic properties of the support were not modified by the addition of Ni but it was concluded to a rearrangement of acid sites. $NiAl_2O_4$ phase leads to an increase of the Lewis acid sites (LAS) of weak strength, generating a decrease of the production of coke and higher catalyst stability. It has been shown that the incorporation of Ni on the Rh/Y-Al catalyst increases the rhodium accessibility and stabilizes the rhodium particles size. Finally, the higher performances of RhNi/Y-Al catalyst were correlated to an increase in the methane steam reforming activity.

1. Introduction

In the current period when renewable energy may be developed, the production of hydrogen from hydrocarbon fuels remains of important interest. Alcohols, and more especially ethanol, are regarded as a possible available power source, and hydrogen production by ethanol steam reforming (ESR) has been extensively studied [1–5]. However, these studies generally deal with the use of pure ethanol and few efforts have been recently performed on the study of hydrogen production from raw bioethanol, i.e. containing impurities. The use of a raw bioethanol feed limits the purification steps and is of major importance for a cost effective industrial application of the ethanol steam reforming process. In a recent paper [6], the effect of impurities present in the raw bioethanol has been studied during ESR reaction in the presence of the Rh/$MgAl_2O_4$ catalyst, developed by Auprêtre et al. [7] for a pure ethanol + water mixture. The impurities chosen for this study, i.e. an acid, an amine, a higher alcohol, an aldehyde and an ester, were representative of the main impurities found in a raw bioethanol feed produced from sugar beet. The study was performed in the presence of pure ethanol containing 1% of one model impurity. It was shown that the impurities can be classified in two categories, corresponding to impurities with either a promoting effect (diethylamine or butanal) or a poisoning effect, leading to the deactivation of the catalyst. The negative effect induced by the presence of impurities can be classified in the following increasing order: acetic acid < butanol < ethyl acetate. Thus, it appeared that the ester and the heavy alcohol are the most deactivating impurities. The effect of the nature of the alcohols has also been studied [8], since alcohols are the most prevailing impurities present in raw ethanol. It was shown that, whereas methanol has no effect on the ethanol steam reforming, the addition of higher alcohols favors the deactivation of the catalyst [9]. The effect is more pronounced with branched alcohols than with linear ones, and the deactivation increases with the amount of carbon atoms in the molecule. Consequently, a molecule such as methyl-2-propan-1-ol can be chosen as model molecule to test the performances of catalysts in the presence of ethanol containing impurities. Whatever the impurity studied, higher alcohol, ester or acid, the deactivation was mainly explained in terms of coke deposition.

* Corresponding author. Tel.: +33 5 49 45 39 97; fax: +33 5 49 45 37 41.
E-mail address: fabien.can@univ-poitiers.fr (F. Can).

0926-3373/$ – see front matter © 2010 Elsevier B.V. All rights reserved.
doi:10.1016/j.apcatb.2010.03.025

Thus, much effort must be focused in the improvement of catalyst formulation in order to increase the coke resistance, especially in presence of impurity.

In the literature, several catalysts have been described for several years. Numerous systems have been studied, using various supports or oxide supported transition metals [10–12]. Noble metals as rhodium supported catalysts have been also largely studied by many authors [13–15]. For instance, Auprêtre et al. [1] showed that Ni and Rh supported on alumina were the most promising catalysts. Besides, there are a lot of evidences in the literature of an improvement in hydrocarbon steam reforming due to the addition of rare earth to the support [16–18]. Thus, the stability of the catalyst for the ESR reaction have been investigated by addition of a wide range of rare earth (RE) elements (Sc, Y, La, Er and Gd) on the Rh/Al_2O_3 base catalyst [19]. It was shown that the RE elements do not have an important impact on the oxidation state and the dispersion of the metallic rhodium centers. It was demonstrated that the catalytic performances of Rh-REOx-Al_2O_3 catalysts are mainly due to the increase of the support basicity and to the rearrangement of acid sites. The presence of a new type of Lewis acid sites (LAS) of weak strength on Rh-REOx-Al_2O_3 materials allows one to decrease the production of coke precursor (C_2H_4). The better result was obtained on catalyst modified by yttrium, named Rh/Y_2O_3-Al_2O_3 material. However, these experiments have been performed using pure ethanol and no reference is available on the catalytic behavior of such a system in presence of impurities.

Otherwise, the use of bimetallic catalysts for hydrogen production from ethanol is of major interest since bimetallic catalysts often show an improved activity and stability compared to their monometallic counterparts [20,21].

Based on these observations, the aim of the present work is to compare the catalytic performances of the reference catalyst $Rh/MgAl_2O_4$ to those of Rh/Y_2O_3-Al_2O_3 and Rh-Ni/Y_2O_3-Al_2O_3 catalysts for the steam reforming of ethanol containing methyl-2-propan-1-ol as model impurity. Samples are characterized by TPR, XRD, IR and carbonaceous deposits produced during the reaction are quantified by TPO.

2. Experimental

2.1. Catalysts

For the reference catalyst $Rh/MgAl_2O_4$, the support was prepared by wet impregnation of a magnesium acetate solution ($Mg(CH_3COO)_2.4H_2O$, Alpha Aesar)) onto γ-Al_2O_3 beads (diameter 1-2 mm, AXENS). The amount of salt was adjusted to obtain 5 wt.% Mg in the support. The spinel structure was obtained by calcination under air at 1000 °C for 15 h [7]

For the modified catalysts, the support was synthesized using the method described in [19]. The alumina beads (diameter 1-2 mm, AXENS) were modified by wet impregnation of yttrium nitrate precursors ($Y(NO_3)_3.6H_2O$). The impregnation was carried out at 45 °C during 48 h under stirring. The solution was then removed using a rotary evaporator, and the beads were let at 120 °C for 15 h and calcined at 900 °C for 15 h at 5 °C min^{-1}. The support is referred as Y-Al.

Monometalic catalysts were prepared using an aqueous rhodium chloride solution ($RhCl_3.3H_2O$) or a nickel nitrate precursor ($Ni(NO_3)_2.6H_2O$) by wet impregnation, respectively for the Rh/Y-Al and the Ni/Y-Al. The bimetallic samples were prepared by wet co-impregnation of rhodium chloride solution and nickel nitrate precursor. The catalysts are referred as RhNi/Y-Al.

Catalysts are finally calcined at 700 °C for 4 h at 2 °C min^{-1}, under air (30 mL min^{-1}).

2.2. Characterization

Mono and bimetallic catalysts were characterized by different techniques, including BET, X-ray diffraction (XRD), temperature programmed reduction (TPR), temperature programmed oxidation (TPO), hydrogen chemisorption and infrared spectroscopy.

Nitrogen adsorption isotherms on the catalysts were performed at–196 °C in a Tristar 3000 Micromeritics apparatus. Prior to the measurement, the samples were pretreated at 250 °C under vacuum for 5 h. The surface area was calculated using the BET method.

Determination of chemical composition was carried out in an ICP-OES Perkin Elmer Optima 2000 DV apparatus. Before the analysis, the samples were prepared using microwave assisted acid (a mixture of HCl and HNO_3) digestion method.

XRD patterns were recorded in a Siemens D5000 diffractometer, equipped with a Cu anode (λ = 0.15406 nm). Diffractograms were recorded in the 15-75° range of 2θ with a step of 0.04° and a dwell time of 6 s. Crystalline phases present in the samples were identified by comparison with ICDD files.

Metal accessibility was determined on Rh/Y-Al, RhNi/Y-Al and Ni/Y-Al with a Micromeritics AutoChem II instrument. Typically, 200 mg of sample were reduced in hydrogen flowing (30 mL min^{-1}) at 400 °C for 1 h, then purged in ultrapure Ar (30 mL min^{-1}) for 2 h and cooled down to room temperature. Pulses of H_2 (0.5347 mL) were injected every minute up to saturation (HC1). A new series of pulses was injected over the sample, after 10 min of purging under pure Ar, to determine the reversible part of the chemisorbed hydrogen (HC2). The irreversible part was taken as HC = HC1–HC2.

Temperature programmed reductions (TPR) were carried out in a Micromeritics AutoChem II apparatus. Before testing, the samples (~250 mg) were calcined from RT to 400 °C at a rate of 20 °C min^{-1} for 15 min in flowing oxygen, in order to eliminated carbonates and residuals species. Catalysts were then cooled down to RT under O_2 (100%, 30 mL min^{-1}) and outgassed under Ar for 30 min (100%, 30 mL min^{-1}). Finally TPR were performed from RT up to 1000 °C at a rate of 5 °C min^{-1} for 30 min under hydrogen flow (1%/in Ar, 30 mL min^{-1}). H_2 consumption was monitored using a TCD.

Temperature programmed oxidation (TPO) were performed after ESR experiments. The used catalyst beads were separated from SiC before analysis. TPO were performed from RT to 1000 °C at a rate of 7 °C min^{-1} under oxygen flow (1%/in He, 12 mL.min^{-1}). At the outlet, pulses of the gas are withdrawn and sent to a TCD detector after separation on a Porapak Q column preceded by a magnesium perchlorate ($Mg(ClO_4)_2$. $6H_2O$) bed in order to trap water. The CO_2 formed by the carbon species oxidation as well as the oxygen consumed are thus analyzed.

Acid-base and metallic properties were characterized by probe molecule adsorption monitored by infrared spectroscopy. Catalysts were pressed into self supported wafers. For acid-base characterization, samples were activated at 450 °C under vacuum in situ in the IR cell. Pyridine or CO_2 probe molecules were adsorbed at room temperature, at various equilibrium pressures (mentioned later) and further desorbed at desired temperature. For the metal phase study, catalysts were reduced under H_2 (150 mL min^{-1}) and evacuated at various temperatures (350, 500 and 650 °C). CO is then adsorbed at ambient temperature. IR spectra were recorded in a Nexus Nicolet spectrometer equipped with DTGS detector (Deuterium TriGlyceride Sulfur) and KBr beam splitter. IR spectra were recorded with a resolution of 4 cm^{-1} and 64 scans. The spectra presented were normalized to a disc of 10 mg cm^{-2}.

2.3. Ethanol steam reforming (ESR) reaction

The apparatus for ethanol steam reforming analysis is described in detail in [7]. The specificity of the feeds depends on the molar

ratio R between ethanol and water, defined as:

$$R = \frac{n_{water}}{n_{ethanol}}$$

Anhydrous ethanol (absolute ethanol VWR) and Ultra-pure water (18.2 MΩ) were used. Catalytic tests were performed by adding 1% (molar percentage) of methyl-2 propan-1-ol as impurity in the water and ethanol mixture, as reported in [6].

The feed was injected with a liquid pump (Gilson 307) in a flow reactor (L = 550 mm; ⌀int = 12.5 mm) made of refractory steel (TP 310 Z15CNS25). The pressure was adjusted by a back pressure regulator (Swagelock). The catalyst sample (0.250 g) was diluted in carborundum (SiC) (2.75 g), with a similar particle size. It was placed in the middle of the reactor, near the temperature controller thermocouple. Void fractions of the reactor were filled with carborundum SiC. The reactor can be fed with pure H_2 or N_2, respectively for catalysis reduction or purging.

The reaction gases were first analyzed on line in a FID Varian after separation on an Alltech AT^{TM}-aquawax column (30m, 0.25 mm). This analysis allowed us to determine the amount of organic compounds present in the reaction flow (ethanol, acetaldehyde...). Then, the reaction gases passed through a condenser at -2 °C to collect water and organic compounds. The flow of gases not condensed at -2 °C (H_2, CO, CO_2, CH_4, C_2H_4, C_2H_6) was measured on line with a Ritter Gas Meters. These gases were then analyzed by a TCD Varian with helium carrier (N_2, O_2, CO and CO_2), by a FID Varian with helium carrier (hydrocarbons compounds) and by an external TCD Perichrom with nitrogen carrier (H_2). The total flow (before condensation) composition was determined using the amount of hydrocarbons compounds as internal standard. These data were recorded every 15 min of ESR reaction. Knowing the concentration of all these products, the calculations enabled us to determine the amount of water converted and the amount of coke formed (calculated as a difference from the carbon balance).

If $n_X{}^{in}$ and $n_X{}^{out}$ are the molar flow rates of the product X at the inlet and the outlet of the reactor, respectively, the catalyst performances are characterized by:

- the product yield (mole of X per mole of introduced EtOH)

$$Y_X = \frac{n_X^{Out}}{n_{EtOH}^{In}}$$

- the carbon balance

$$\text{C balance} = \frac{\sum \chi . n_X^{out}}{2 . n_{EtOH}^{in}} \times 100$$

where χ is the stoichiometry factor (corresponding to the number of C present in the compound).

- the ethanol conversion

$$X_{EtOH} = \frac{n_{EtOH}^{In} - n_{EtOH}^{Out}}{n_{EtOH}^{In}} \times 100$$

- the selectivity in CO_2/COx compounds

$$S_{CO2/COx} = \frac{n_{CO2}^{out}}{n_{CO}^{out} + n_{CO2}^{out}} \times 100$$

The reaction is performed at 675 °C and 2 bar. The molar ratio R is fixed at 4. The flow rate of the liquid feed (ethanol + water, R = 4) is fixed to 0.23 mL min^{-1}, which corresponds to a WHSV (Weight Hourly Space Velocity) of 19.5 h^{-1} (ethanol weight flow/weight of catalyst). Before catalytic test, the catalyst sample was reduced from ambient temperature to the reaction temperature (675 °C) during 4 hours under H_2 (150 mL min^{-1}) with a temperature ramp of 10 °C min^{-1} and then flushed under N_2 (150 mL min^{-1}) in order to purge hydrogen. Then, the gas flow was stopped and the reaction was started by introduction of the ethanol and water mixture onto the catalyst.

3. Results

3.1. Catalytic behavior

3.1.1. Effect of methyl-2-propan-1-ol impurity in ethanol steam reforming reaction

Generally, the steam reforming reaction is studied using pure ethanol and water mixture. A first work [19] was focused on the increases of the catalytic behavior by addition of rare earth element of the alumina support, namely Rh/Y_2O_3-Al_2O_3 (i.e, Rh/Y-Al). Without impurities, it has been shown that the ethanol conversion, the stability and the hydrogen production are extensively increased with the Rh/Y-Al catalyst compared to the reference sample Rh/$MgAl_2O_4$ [9]. With the addition of a second metal (RhNi/Y-Al), results obtained with pure ethanol and water mixture (results not shown) are quite similar to that of the monometallic sample (Rh/Y-Al). In this work, the effects of the model impurity, methyl-2-propan-1-ol on the catalytic behavior of different samples were more specially investigated. Results obtained with Ni supported Y_2O_3-Al_2O_3 (Ni/Y-Al catalyst) are not presented, since a strong deactivation was observed with this sample in the first hours of catalytic test.

Usually, the ethanol steam reforming results in three main reactions accounting for the formation of CO, CO_2, H_2 and CH_4:

$$C_2H_5OH + 3H_2O \rightarrow 2CO_2 + 6H_2 \quad \Delta H^\circ_{298} = +174\,\text{kJ.mol}^{-1} \quad (1)$$

$$C_2H_5OH + H_2O \rightarrow 2CO + 4H_2 \quad \Delta H^\circ_{298} = +256\,\text{kJ.mol}^{-1} \quad (2)$$

$$C_2H_5OH + H_2 \rightarrow 2CH_4 + H_2O \quad \Delta H^\circ_{298} = -175\,\text{kJ.mol}^{-1} \quad (3)$$

Nevertheless, simultaneous reactions can occur in which essentially acetaldehyde and ethylene may be produced, by ethanol dehydrogenation (4) and ethanol dehydration (5) [1,3]:

$$CH_3\text{-}CH_2\text{-}OH \rightarrow CH_3\text{-}CH = O + H_2 \quad (4)$$

$$CH_3\text{-}CH_2\text{-}OH \rightarrow CH_2 = CH_2 + H_2O \quad (5)$$

Note that the ethylene formation leads to the deactivation of the catalyst, since it is regarded as a coke precursor (polymerization reaction (6)) [22,23].

$$C_2H_4 \rightarrow \text{polymers} \rightarrow \text{coke} \quad (6)$$

It was shown in [6] that the dry gas (H_2, CO_2, CO, CH_4, reaction (1), (2), (3) and (4)) flowrate can be correlated to the catalytic activity. Thus, the evolution of the dry gas flowrate can be reported as a function of time on stream (TOS) to have a direct idea on the stability of the catalysts. The evolution of the dry gas flowrate as a function of TOS during ESR in the presence of methyl-2 propan-1-ol is illustrated in Fig. 1 for the Rh/$MgAl_2O_4$, Rh/Y-Al and RhNi/Y-Al catalysts, and the performances of the catalysts are presented in Table 1.

Firstly, Fig. 1 shows that the dry gas flowrate decreases very strongly with the Rh/$MgAl_2O_4$ sample leading to an important deactivation of the catalyst. On the contrary, no deactivation is observed on the catalysts supported on Y_2O_3-Al_2O_3 and the bimetallic sample presents the most important dry gas flowrate. According to these results, conversions of ethanol reported in the Table 1 after 8 h of TOS also show a weak activity of the Rh/$MgAl_2O_4$ sample compared to catalysts supported on Y_2O_3-Al_2O_3 (56.0%,

Table 1
Effect of the metallic phase on the catalytic performances (Yield in major products, ethanol conversion and amount of coke deposit) during ethanol steam reforming in the presence of methyl-2 propan-1 ol impurity at 675 °C; P=2Bar; R=4; $WHSV_{EtOH}$=19.5 h^{-1}. In italics: molar percentage.

	gas composition (mol mol^{-1}) and percentage of each species[a]								X_{EtOH} (%)[b]	CO_2/COx	Coke[c] mgC.g_{cata}^{-1}
	H_2	CO	CO_2	CH_4	C_2H_4	C_2H_6	CH_3CHO	H_2O			
Thermodynamic equilibrium	3.77 *42.8%*	0.54 *6.1%*	0.71 *8.1%*	0.10 *1.1%*	-	-	-	3.03 *34.5%*		*56.8%*	
$Rh/MgAl_2O_4$	1.05 *18.9%*	0.31 *5.6%*	0.10 *1.8%*	0.29 *5.2%*	0.11 *2.0%*	0.04 *0.7%*	0.05 *0.9%*	3.61 *64.9%*	56.0	*24.4%*	62.5
Rh/Y-Al	3.53 *42.2%*	0.70 *8.4%*	0.72 *8.6%*	0.55 *6.6%*	0.01 *0.1%*	0.01 *0.1%*	0.01 *0.1%*	2.84 *33.9%*	97.2	*50.7%*	12.4
RhNi/Y-Al	3.84 *44.9%*	0.75 *8.8%*	0.76 *8.9%*	0.46 *5.4%*	0.01 *0.1%*	0.01 *0.1%*	0.01 *0.1%*	2.71 *31.7%*	98.2	*50.3%*	3.5

[a] average after 8 hours of time on stream. Standard deviation: ± 4%.
[b] conversion measured after 8 hours of time on stream.
[c] measured from the TPO experiments (type II + type III + type IV).

97.2% and 98.2% for the $Rh/MgAl_2O_4$, Rh/Y-Al and RhNi/Y-Al catalysts, respectively). The strong deactivation of the reference sample $Rh/MgAl_2O_4$ and the weak conversions of ethanol are generally assigned in the literature to the carbonaceous species [9]. The coke production results from the ethylene formation and one can note that the C_2H_4 amount is very high for the $Rh/MgAl_2O_4$ catalyst. On the contrary, the production of ethylene is low for the metallic catalysts supported on Y_2O_3-Al_2O_3 material. It does not exceed 0.01 mol/mol of introduced ethanol for the Rh/Y-Al and RhNi/Y-Al samples compared to 0.11 mol/mol for the $Rh/MgAl_2O_4$ catalysts.

Data listed in Table 1 show that the CH_4 level is higher than the value given at the thermodynamic equilibrium, whatever the catalyst. This result suggests that (i) methane may be a primary product as already suggested in [5] even if methane may also be a secondary product resulting from CO hydrogenation and (ii) that our catalysts are not very active for methane reforming. Methane may also be produced by acetaldehyde decarboxylation (7) reactions leading to the production of methane and CO:

$$CH_3\text{-}CH = O \rightarrow CH_4 + CO \quad (7)$$

Besides, it has been reported in [19] that contrary to what was observed by Pettigrew et al. [24], the presence of rare earth element as Yttrium does not favor the methanation reaction (8) of CO by H_2, in our applied conditions, especially of temperature.

$$CO + 3H_2 \leftrightarrow CH_4 + H_2O \quad (8)$$

Then, it can be considered that methane is not produced by hydrogenation of carbon monoxide in the presence of our catalysts and in the chosen experimental conditions but is likely to be a primary product that is then converted to yield hydrogen by steam reforming. One can note some differences concerning the methane production for the Rh/Y-Al and the RhNi/Y-Al samples. In fact the RhNi/Y-Al catalyst leads to the lower production of CH_4, with 0.46 mol/mol compare to 0.55 mol/mol for the Rh/Y-Al. The amount of water presented in Table 1 is also different on these two catalysts. A tentative explanation may be put forward by the higher activity in methane steam reforming reaction of the RhNi/Y-Al sample. This assumption explains the higher H_2 yield and the lower CH_4 and H_2O yield, obtained with the RhNi/Y-Al sample, according to the equation (8). Finally, one can note that the methane steam reforming reaction also leads to a production of CO. This can explain the higher carbon monoxide yield observed in Table 1 for the catalyst modified by nickel incorporation.

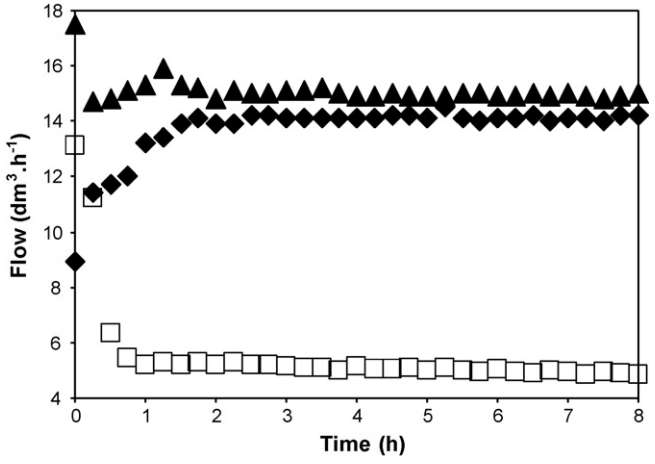

Fig. 1. Dry gas flowrate as a function of time on stream obtained during the ESR reaction with 1% of methyl-2-propan-1-ol impurity over the $Rh/MgAl_2O_4$, Rh/Y_2O_3-Al_2O_3 and $RhNi/Y_2O_3$-Al_2O_3 catalysts (675 °C, 2 bar, *R* = 4). (□): $Rh/MgAl_2O_4$; (♦): Rh/Y-Al; (▲): RhNi/Y-Al.

The CO production can likewise be correlated to the CO_2 yield by the water gas shift (WGS) reaction that can be assessed using the CO_2/COx ratio reported in Table 1 (reaction 9):

$$CO + H_2O \leftrightarrow CO_2 + H_2 \quad (9)$$

The activity of catalysts in the WGS reaction is known to be enhanced by the presence of rare earth elements in the support, as reported in the literature [19,25–29]. Results reported in Table 1 indicate that the modification of the support by yttrium incorporation extensively increases the CO_2/COx ratio, from 24.4% to 50.7% and 50.3%, for the $Rh/MgAl_2O_4$, Rh/Y-Al and the RhNi/Y-Al catalysts, respectively. The higher performances of the yttrium doped materials for the WGS reaction may explain the high H_2 yield observed for the Rh/Y-Al and the RhNi/Y-Al catalysts. However, for these two catalysts supported on Y-Al, the CO_2/COx ratio is similar, whereas the hydrogen yield is higher on the bimetallic catalyst. Then, it can be inferred that the supplementary hydrogen yield is produced by higher activity in the methane steam reforming reaction of the RhNi/Y-Al sample.

At last, in order to understand the higher stability of the Y-Al supported samples compared to the $Rh/MgAl_2O_4$ reference catalyst, temperature-programmed oxidation (TPO) experiments were carried out to identify the carbon species deposited on the surface of the various catalysts during the steam reforming reaction with impurity.

3.1.2. Temperature-programmed oxidation (TPO)

Firstly, the thermal stability of accumulated carbon have been studied by temperature programmed desorption (TPD) and reveals that an insignificant amount of CO_2, assigned to carbonates species, is desorbed. The CO_2 response recorded during the TPO of accumulated carbon over modified catalysts is reported in Fig. 2. These TPO experiments were performed on the spent catalyst, after 8 h of ESR in the presence of methyl-2 propan-1-ol as impurity. As already mentioned in detail in [19], 4 types of coke can be oxidized at different temperatures, with maxima at roughly (I) 310 °C, (II) 380 °C, (III) 520 °C and (IV) 695 °C. In accordance with the reactivity of the carbon species formed during the ESR reaction, the first peak (I) was ascribed to coke deposited on metallic centers [30].

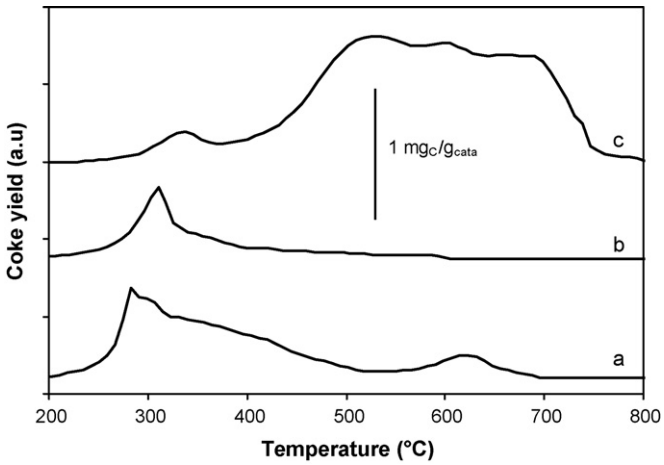

Fig. 2. Temperature-programmed oxidation (TPO) of carbon species formed after 8 h of ESR reaction with 1% of methyl-2-propan-1-ol impurity, over: (a) Rh/Y-Al; (b) RhNi/Y-Al; (c) $Rh/MgAl_2O_4$.

The second peak can be assigned to coke deposited near the metal-support interphase. The peak III was ascribed to coke deposited on the support. The fourth one is less reactive and is oxidized at high temperature, which suggests that this type of carbon mainly exists as graphite phase, formed during the ESR reaction and generated by the thermal ethanol decomposition pathway [18,31].

The TPO profiles (Fig. 2) show that the proportion and the reactivity of each type of carbon (I, II, III, IV) is altered, firstly by the presence of yttrium introduced in the support, and secondly by the Ni deposition. The peaks II and III are present only on the $Rh/MgAl_2O_4$ catalyst. One can note that the type IV carbon species, which corresponds to the oxidation of the most stable carbon species, is not observed on the sample modified by Ni incorporation, which is otherwise the most active in ESR reaction. The amount of coke deposited on catalyst during the reaction measured from TPO experiments are reported in Table 1 (type II + type III + type IV). It appears that the carbonaceous deposit is also the lowest on the RhNi/Y-Al catalyst. This result is in agreement with the whole data displayed in Table 1. In fact, hydrogen production, stability and coke resistance are increased with the incorporation of the nickel in the Rh/Y-Al catalyst, even with 1% of methyl-2-propan-1-ol as impurity. Then, a relationship can been reported in Fig. 3 between the

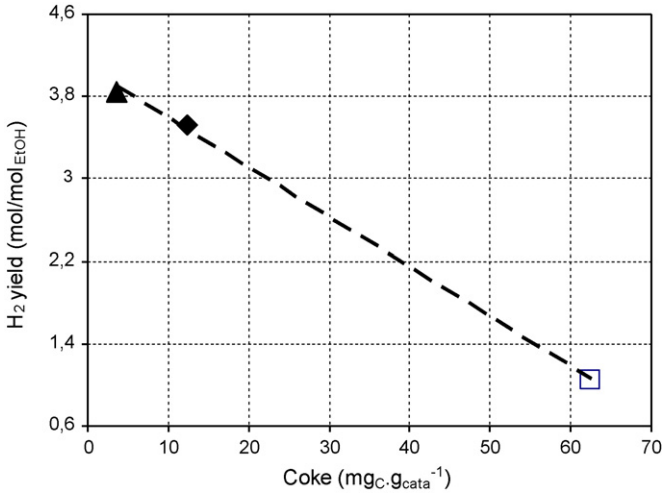

Fig. 3. Relationship between the hydrogen yield and the carbon deposited (type II, III and IV) during the ESR reaction with 1% of methl-2-propan-1-ol impurity. (□): $Rh/MgAl_2O_4$; (♦): Rh/Y-Al; (▲): RhNi/Y-Al.

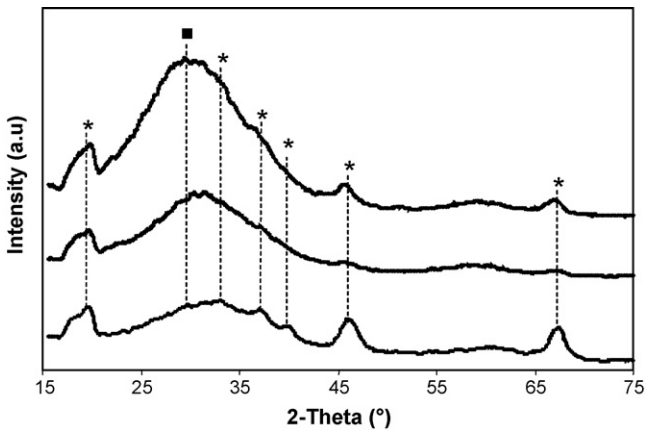

Fig. 4. XRD patterns of mono and bi-metallic catalysts supported on Y_2O_3-Al_2O_3. (a) Rh/Y-Al; (b) Ni/Y-Al; (c) RhNi/Y-Al. (*): θ-Al_2O_3; (■): Y_2O_3.

hydrogen yield recorded during the ESR and the amount of carbon deposited after the catalytic test (type II, III and IV), displayed in Table 1. One can note (Fig. 3) that the higher the hydrogen yield, the lower the carbon amount deposited on the sample. Then, the RhNi/Y-Al and the Rh/Y-Al samples, which are the most active catalysts for the ESR with 1% of methyl-2-propan-1-ol as impurity, present also the lowest amount of carbonaceous species. Thus, the better catalytic behavior observed with the RhNi/Y-Al sample may be assigned likewise to a better coke resistance, and therefore to a slower deactivation.

Finally, in order to understand the effect of Ni, the RhNi/Y-Al catalyst has been thereafter characterized and compared to the Rh/Y-Al reference sample. The surface properties of the Ni/Y-Al material were also investigated. Physical and chemical properties of the catalysts were studied using BET, infrared spectroscopy, TPR and XRD analysis.

3.2. Characterization

3.2.1. Physical and chemical properties of the catalysts

In Table 2 are reported the BET surface areas, the metal content and the amount of chemisorbed hydrogen (HC) for the Ni/Y-Al, Rh/Y-Al and RhNi/Y-Al catalysts.

The values of the hydrogen chemisorption (HC) of the monometallic samples reported in Table 2 are strongly different. For the Rh/Y-Al sample, the HC is about 28.1 $\mu mol\,g^{-1}$, whereas the Ni/Y-Al does not chemisorb H_2 in our experimental conditions (0.17 $\mu mol\,g^{-1}$). Nevertheless, the amount of HC presented in Table 2 shows that the addition of Ni to the Rh/Y-Al sample strongly increases the consumption of H_2. This result obtained for the RhNi/Y-Al sample may be due to a higher rhodium and/or nickel dispersion in the bimetallic. This last point will be discussed latter.

For the monometallic samples, the data compiled in Table 2, show a similar BET specific surface area, with 136 and 133 $m^2\,g^{-1}$ for the Ni/Y-Al and the Rh/Y-Al catalysts, respectively. The bimetallic catalyst shows a specific surface area slightly lower, of 110 $m^2\,g^{-1}$, than those of the monometallic samples. Moreover, one can note from the ICP-OES results (Table 2) that the nickel content is more important in the bimetallic catalyst. It appears that the higher the nickel loading, the lower the specific surface area, indicating a possible blockage of the pore volume by nickel incorporation.

In order to understand the effect of Ni addition on physical properties of the bimetallic catalysts (RhNi/Y-Al), XRD and TPR experiments were performed.

The structure of synthesized catalysts was studied by X-ray diffraction. Diffractograms are presented in Fig. 4. The XRD patterns

Table 2
Characteristics of Rh, Ni and Rh-Ni catalysts supported on Y_2O_3-Al_2O_3.

Catalysts	BET Surface area ($m^2\ g^{-1}$)	Metal loading (ICP) (wt %)		H_2 chemisorbed ($\mu mol.g^{-1}$)
		Rh	Ni	
RhNi/Y-Al	110	0.82	6.12	45.22
Ni/Y-Al	136	-	4.80	0.17
Rh/Y-Al	133	0.94	-	28.13

of the alumina modified-supported rhodium catalysts (Rh/Y-Al) was already described in [19], and showed an outbreak of segregation of an additional phase resulting from the impregnation of rare earth elements to the parent alumina (2θ = 25-35°). However, one can note that the XRD patterns are not very well defined and that the addition of nickel to Y-Al oxide (Ni/Y-Al) or rhodium supported catalyst (RhNi/Y-Al) does not produce any observable shift in the XRD reflections. Finally, no Rh phase was detected by XRD on any of the samples, presumably because the metal content and the metallic particle sizes are too small.

Temperature programmed reduction (TPR) profiles displayed in Fig. 5 strongly differ from a catalyst to another. The Rh/Y-Al sample shows one peak at about 90 °C, labeled A, typically assigned to the reduction of the rhodium phase, as already reported in numerous papers [32–34]. For RhNi/Y-Al, TPR profile also exhibits one peak at about 112 °C (labeled A), which could correspond to the reduction of rhodium alone. However, this reduction temperature being higher than that observed on the monometallic Rh/Y-Al catalyst, either Rh is much more dispersed in the bimetallic than in the monometallic catalyst, or rhodium is in interaction with nickel. In the RhNi/Y-Al, additional peaks are also observed at about 350–475 °C (labeled B and C) and at about 850 °C (labeled D). In the literature, it has been reported that for samples with high Ni content (Ni ≥ 0.3% molar), the aggregated NiO particles are so big that they cannot be reduced completely in one step. Therefore, it can be seen that the reduction of NiO occurs as following: $NiO \rightarrow Ni^{\delta+} \rightarrow Ni^0$, respectively at 400 °C and 550 °C [35]. The association between Ni and a support, such as alumina significantly affects the reducibility of NiO, which usually results in the shift of its reduction peaks [36], that explain the temperature of reduction peaks observed in Fig. 5. The reduction peaks observed at higher temperature (850 °C, labeled D in Fig. 5) is typical of Ni/alumina catalysts containing $NiAl_2O_4$ spinel phase [37,38]. The presence of this phase is not supported by XRD analysis (Fig. 4) in which no peak corresponding to $NiAl_2O_4$ was evidenced. The interaction between nickel and the alumina support is complex. During preparation Ni^{2+} could disperse on the surface of Al_2O_3, or diffuse into the bulk structure of the support to different extents, depending on the intrinsic properties of the support, nickel loading, and preparation parameters. Nickel can be highly dispersed on the surface and incorporated into the spinel structure of alumina to form a diluted $NiAl_2O_4$-like phase that is not observable in XRD patterns [37,38]. From the values of the ratio H_2/Ni reported in Table 3 given for peaks (B + C) and peak D, one can calculate the proportion of each type of nickel species which are equal to 40% for the dispersed nickel phase and 60% for the nickel aluminate. As before the catalytic test, the catalyst is activated by reduction at 675 °C, one can note that nickel dispersed at the support surface is totally reduced at the beginning of the ethanol steam reforming reaction.

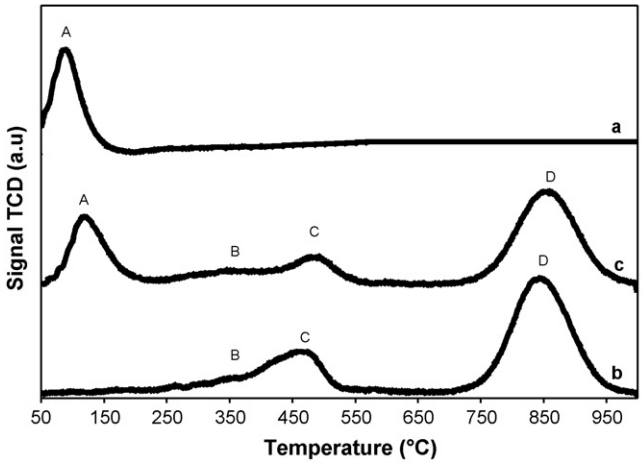

Fig. 5. TPR profiles of mono and bi-metallic catalysts supported on Y_2O_3-Al_2O_3. (a) Rh/Y-Al; (b) Ni/Y-Al; (c) RhNi/Y-Al.

Values of H_2/Ni ratio, corresponding to H_2 consumption measured by TPR experiments related to peak B, C and D (Table 3), involve the following reactions for the reduction of Ni^{2+} species:

$$NiO + H_2 \rightarrow Ni + H_2O.$$

$$NiAl_2O_4 + H_2 \rightarrow Ni + H_2O + Al_2O_3$$

Then, theoretically, both reactions need one hydrogen molecule per Ni atom. As the total amount of H_2 needed to reduce nickel oxide to metallic Ni (Peaks B + C + D) is nearly equal to a H_2/Ni of 1 (Table 2), it can be inferred that all the nickel present in the catalyst is in the Ni^{2+} form and is reduced from 200 °C. This shows that the reduction peak observed around 90 °C on Rh/Y-Al and RhNi/Y-Al catalysts can be assigned only to the reduction of the rhodium, and may be regarded as a result of the following reduction reaction:

$$RhO_x + xH_2 \rightarrow Rh + xH_2O.$$

The temperature at the maximum of this peak slightly differs on rhodium supported catalyst (curves a and c, Fig. 5): 90 °C for the Rh/Y-Al sample and 112 °C for the RhNi/Y-Al sample. This difference may be assigned to the presence of RhOx nanocrystallites with different sizes [32,33]. It appears that the presence of nickel increases the temperature of H_2 consumption assigned to rhodium reduction, which may be explained by a higher rhodium dispersion on the support surface. This result is in agreement with the higher amount of chemisorbed hydrogen recorded in the RhNi/Y-Al sample compared to the Rh/Y-Al catalyst (Table 2).

The values of the H_2/Rh ratio reported in Table 3 enable to determine the nature of rhodium species at the surface of the catalyst. On supported catalysts, the most common species quoted in the literature is Rh_2O_3 [39,40]. This corresponds to the higher oxidation state of rhodium (+III), and leads to a H_2/Rh ratio equal to 1.5. Taking into account the rhodium content in our catalysts, the theoretical hydrogen consumption for the complete reduction of Rh_2O_3 should be of 120 $\mu mol\ g^{-1}$ and 137 $\mu mol\ g^{-1}$, for the RhNi/Y-Al and the Rh/Y-Al samples, respectively, whereas the experimental values are equal to 170 and 198 $\mu mol\ g^{-1}$ respectively (Table 3). These data show that the H_2 consumed to reduce RhOx species exceeds the amount of H_2 needed to reduce Rh_2O_3 to metallic Rh. This lead to a H_2/Rh ratio higher than 1.5 (respectively 2.2 and 2.1 for Rh/Y-Al and RhNi/Y-Al), suggesting that some of the surface oxygen on Y_2O_3-Al_2O_3 support may be reduced in addition to the oxidized Rh, as it has already been reported for redox materials in [41].

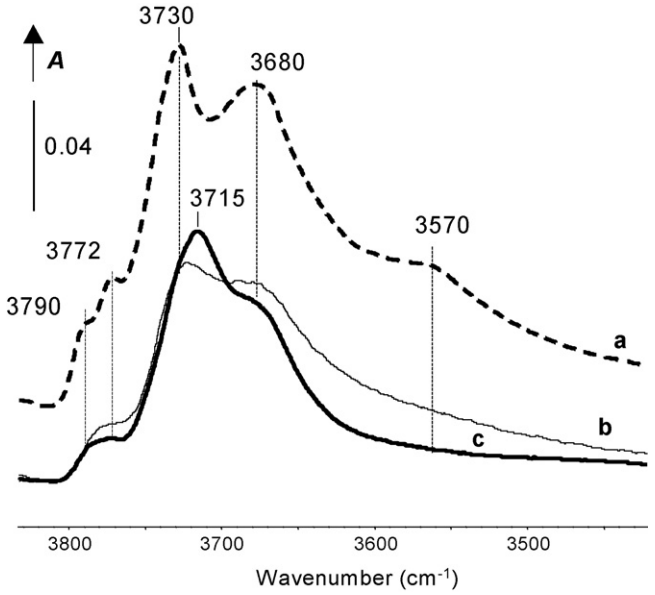

Fig. 6. IR spectra in the ν(OH) region of catalysts activated by outgassing at 450 °C. (a) Rh/Al (in dotted line); (b) Rh/Y-Al; (c) RhNi/Y-Al.

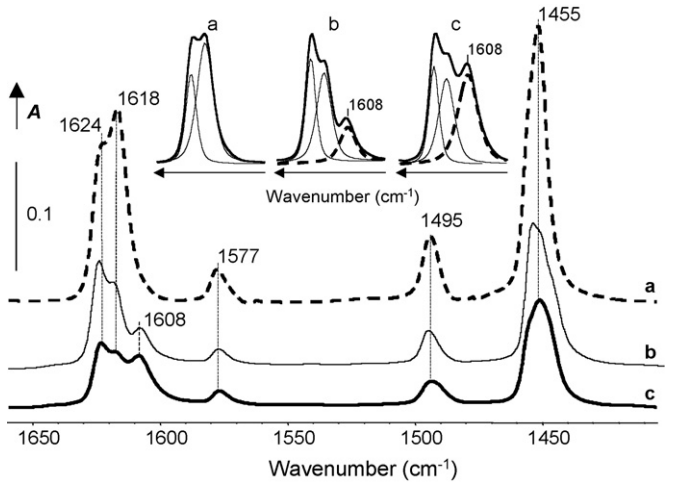

Fig. 7. (A): IR difference spectra of pyridine desorbed at 200 °C. In insert: IR decomposition peaks in the ν_{8a} range of pyridine desorbed at 200 °C. (a) Rh/Al (in dotted line); (b) Rh/Y-Al; (c) RhNi/Y-Al.

3.2.2. Infrared study

In this part, the effects of Ni addition on the surface properties of the catalysts are studied. In this way, acid base properties, as well as residual OH groups of alumina support, were investigated using pyridine and CO_2 adsorption monitored by IR spectroscopy, respectively on Rh/Y-Al and RhNi/Y-Al. In order to compare and also observe the effect of yttrium toward alumina, this study was expanded on the Rh/Al sample. In a second way, metallic properties were characterized by CO adsorption. The Rh/Al material is not presented since the results obtained are similar to those of the Rh/Y-Al sample. Results obtained on the Ni/Y-Al are also shown in order to understand the effect of Ni on the RhNi/Y-Al catalyst.

3.2.2.1. Surface properties. In Fig. 6, the IR spectra in the OH stretching region of pure alumina, mono and bimetallic supported sample on modified support were compared after outgassing at 450 °C. The IR spectrum of Rh/Al reference catalyst (spectrum a in dotted line, Fig. 6) is consistent with that reported in the literature [42], showing the different types of OH groups of alumina that display bands at 3790, 3772, 3730 and 3680 cm^{-1}. A broader band is also detected whose maximum is centered near 3570 cm^{-1}, due to H-bonded of adsorbed water. This could be explained by the dissociation of atmospheric water on Lewis acid sites (LAS) of alumina. However, one can note that this band is less visible on the Rh/Y-Al sample (spectrum b, Fig. 6) and is not present on RhNi/Y-Al (spectrum c, Fig. 6). As this species results from the presence of LAS, one can expect a lower acidic character of these metallic samples.

The spectra of Rh supported samples (Rh/Y-Al and RhNi/Y-Al) are significantly different for the free OH groups. The band at 3730 cm^{-1} evidenced on the Rh/Al sample is the most affected by the addition of yttrium on the alumina support and is almost disappeared on the RhNi/Y-Al catalyst (spectra c, Fig. 6). Conversely, there is one band clearly evident which appears with maximum at 3715 cm^{-1}. In the literature [43], it has been related that the IR spectrum of $NiAl_2O_4$ in OH stretching region shows three bands near 3790, 3720 and 3670 cm^{-1}. They fall in the usual region of free hydroxyl group of alumina, but the extent of the new band observed at 3715 cm^{-1} for RhNi/Y-Al catalyst is in accordance with the presence of a spinel structure [43] such as $NiAl_2O_4$. This result confirms those previously reported for the temperature programmed reduction experiments. Finally, the addition of yttrium to Rh/Al parent sample leads to the decrease of the amount of the acidic type III OH groups (ν(OH) at 3680 cm^{-1}), as already reported for other dopes [44].

3.2.2.2. Acid-base properties. Firstly, the surface acidity was evaluated by IR spectroscopy of adsorbed pyridine. After activation at 450 °C, pyridine was adsorbed (200 Pa at equilibrium) at room temperature and further desorbed at 200 °C (by temperature step of 50 °C), in order to eliminate physisorbed and H-bonded pyridine from the surface. IR spectra are presented in Fig. 7. Acidity is monitored by the ring vibration modes ν8a, ν8b, ν19a and ν19b of adsorbed pyridine, as studied by Parry [45]. IR adsorption band on Rh/Al (spectrum a, Fig. 7) are then observed at 1624, 1618, 1577, 1495 and 1455 cm^{-1}, assigned to coordinated pyridine on Lewis acid sites (LAS). No IR band assigned to pyridinium was observed, as expected on alumina which does not present OH groups strong enough to protonate the pyridine.

Generally, two preferential vibration modes are studied in order to probe the LAS strength and concentration by pyridine adsorption. The ν19b allows one to quantify the total amount of coordinated pyridine, obtained from the surface area of this absorption band, using its molar coefficient ($\varepsilon_{\nu 19b}$ = 1.5 cm μmol^{-1} [46]). The ν8a enables to discriminate the strength of LAS.

Table 3
Hydrogen Temperature Programmed Reduction (TPR) results of Rh, Ni and Rh-Ni catalysts supported on Y_2O_3-Al_2O_3.

Catalysts	H_2 consumption ($\mu mol\ g^{-1}$)			H_2/M^* ratio			
	Peak (A)	Peaks (B+C)	Peak (D)	Peak (A)	Peaks (B+C)	Peak (D)	Peaks (B+C+D)
Rh/Y-Al	198	-	-	2.2	-	-	-
RhNi/Y-Al	170	453	673	2.1	0.44	0.65	1.09
Ni/Y-Al	-	381	569	-	0.47	0.70	1.17

* M: Rh or Ni.

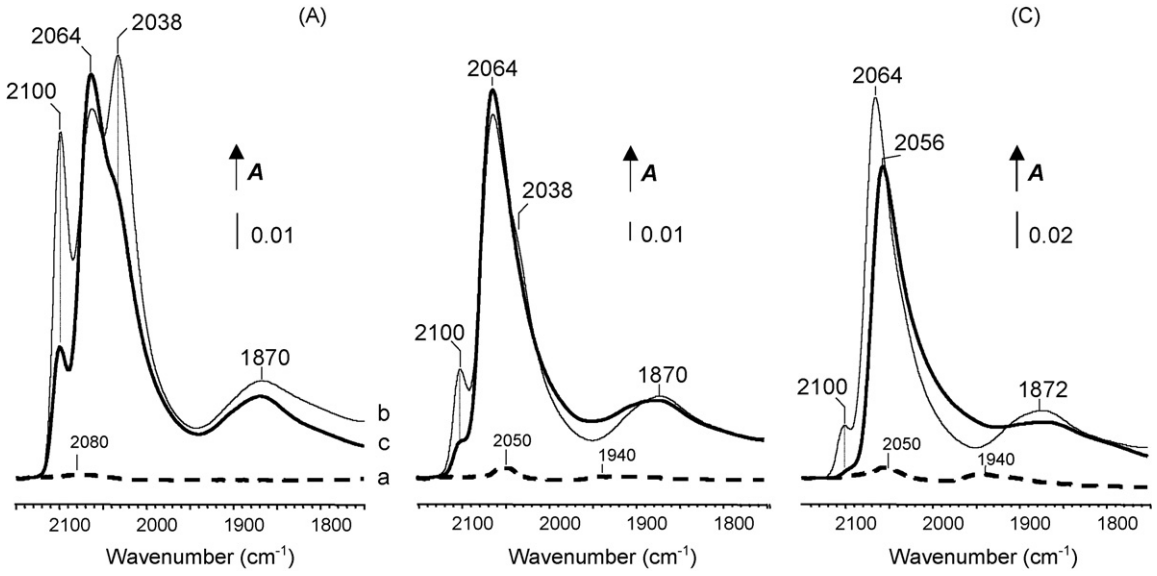

Fig. 8. IR difference spectra of CO adsorbed at ambient temperature (8 μmol) of catalysts initially reduced at A: 350 °C; B: 500 °C; C: 650 °C. (a) Ni/Y-Al; (b) Rh/Y-Al; (c) RhNi/Y-Al.

IR spectra of pyridine adsorbed on alumina support have been largely studied since several years [47,48]. Indeed, for the Rh/Al catalyst (spectrum a, Fig. 7), two bands can be distinguished in the ν8a range at 1624 and 1618 cm^{-1}, assigned to pyridine coordinated to tetrahedral Al^{3+} (strong LAS) and to both tetrahedral and octahedral Al^{3+} (medium LAS). For Rh supported on the alumina modified by addition of yttrium (spectra b and c, Fig. 7), an additional band is observed at 1608 cm^{-1} as related in [19]. In agreement with previous works [49,50], this band is assigned to pyridine adsorbed on weak coordinatively unsaturated sites (cus) of rare earth ions located on the alumina surface. However, for the RhNi/Y-Al sample, this supplementary band may also be assigned to pyridine coordinated over Ni^{2+} in the spinel structure, since Busca et al. [51] observed also a band at 1605 cm^{-1} on their $NiAl_2O_4$ support.

The occurrence of ν8a mode at three frequencies may indicate the presence of LAS with different strength. The deconvolution of peaks in this spectral region may be used to describe the heterogeneity of LAS of each sample. Results are presented by the inserted spectra in Fig. 7. They display that RhNi/Y-Al sample presents the higher relative amount of weak LAS. The concentration of each type of LAS is reported in Table 4, using the total amount of coordinated pyridine evaluated by the area of ν19b band evacuated at 200 °C. As described above, the Rh/Al sample does not present the weak LAS assigned to the pyridine absorption band at 1608 cm^{-1}.

The addition of yttrium to Al_2O_3, and then of the nickel decrease the total amount of LAS, from 97.3 μmol g^{-1} for the Rh/Al to 51.9 and 41.1 μmol g^{-1} for the Rh/Y-Al and the RhNi/Y-Al samples, respectively (Table 4). These results show that the integration of Ni slightly decreases the total acidity compared to the Rh/Y-Al sample. The addition of yttrium to alumina affects both the medium and strong LAS. The medium LAS are less affected by the integration of Ni to the Y-Al sample, compared to the addition of yttrium to the Al support. The presence of a new type of LAS of weak strength is observed on Rh/Y-Al and RhNi/Y-Al, and the amount of this one is increased by the Ni integration to the Rh/Y-Al catalyst. This result may be assigned to the presence of a $NiAl_2O_4$ spinel structure on the RhNi/Y-Al sample, leading to Ni^{2+} cus which present a lower acidic character. One can note that the addition of Ni strongly decreases the amount of strong LAS compared to the monometallic catalyst.

Basic properties of materials were then characterized by carbon dioxide adsorption monitored by FTIR spectroscopy. It was previously observed that the yttrium addition to the alumina support strongly alter the basic properties of the support. Spectra are not presented here, but it was established that bands assigned to hydrogen carbonates species diminish, indicating that the addition of yttrium decreases the concentration of surface OH groups, as evidenced previously in Fig. 6. The addition of yttrium leads to the appearance of two bands near 1600 and 1333 cm^{-1}, corresponding to a $\Delta\nu_3$ splitting of 267 cm^{-1}, assigned to a bidentate carbonate interacting with medium basic sites, as those associated with a metal cation such as a rare earth element as yttrium [19]. Obvious modifications are not observed about the amount and the nature of carbonate structure with the introduction of Ni to the catalyst. The basic properties induced to yttrium are then maintained even in the RhNi/Y-Al sample.

3.2.2.3. Metallic properties. Metallic properties of rhodium and rhodium-nickel supported catalysts were investigated using CO adsorption monitored by IR spectroscopy. Samples were firstly reduced under hydrogen flow (150 mL min^{-1}, 1 hour) and then evacuated at the desired temperature, i.e.: 350 °C, 500 °C and 650 °C. Carbon monoxide was then adsorbed at ambient temperature. For better understanding, the Ni/Y-Al sample was also characterized following the same experimental procedure. Spectra are reported in Fig. 8.

In the literature, much attention has being paid to the study of CO infrared data on Rh/Al_2O_3 supported catalysts. Depending on the Rh loading and the reduction conditions, mainly three kinds of carbonyl species have been reported [52]. The first species is characterized by one band observed at ν(CO) around 2060 cm^{-1} and the second species by a broad band between 1800 and 1900 cm^{-1}. The former band is due to linear monocarbonyl species leading to CO adsorbed on top of a Rh atom (RhCO). The latter band is due to CO bridged on two Rh atoms (Rh_2CO). The third species consists in the geminal dicarbonyl ($Rh^I(CO)_2$), characterized by symmetric and antisymmetric $\nu(CO)_2$ stretching modes (observed in the literature at 2095 and 2027 cm^{-1}, respectively), which strongly differs from the monocarbonyl species that present a single ν(CO) mode.

Fig. 8 shows the 2150-1750 cm^{-1} region of the infrared spectra of 8 μmol of CO adsorbed on catalysts reduced at various temperatures (350 °C, 500 °C and 650 °C). The CO adsorption on Ni/Y-Al catalyst initially reduced at 350 °C (spectrum a, Fig. 8A) leads to a small band at about 2080 cm^{-1}, which falls at lower frequencies with respect to the gas phase CO that involves carbonyls formation

Table 4
Concentration of each type of LAS after evacuation of pyridine at 200 °C (μmol g^{-1}).

Catalysts	weak LAS (ν8a=1608cm^{-1})	medium LAS (ν8a=1618cm^{-1})	strong LAS (ν8a=1624cm^{-1})	Total
Rh/Al	0	64.9	32.4	97.3
Rh/Y-Al	9.6	23.7	18.5	51.9
RhNi/Y-Al	18.6	14.2	8.3	41.1

on cations having d-type electrons, such as Ni^{2+} or more reduced Ni centers [43]. The presence of oxidized Ni confirms that a temperature of 350 °C is not sufficient to reduce Ni, in accordance with the TPR results. For higher reduction temperatures (Fig. 8 B and C), new bands at 2050 and 1940 cm^{-1} were observed characterizing $Ni^0(CO)$ and $Ni_2(CO)$ [53].

For rhodium supported catalysts (Rh/Y-Al), carbonyl species described above were observed in Fig. 8, namely linear monocarbonyl (νCO at 2064 cm^{-1}), bridged carbonyl (νCO at 1870-1872 cm^{-1}) and geminal dicarbonyl species (ν_sCO at 2100 cm^{-1}; ν_{as}CO at 2038 cm^{-1}). The formation of dicarbonyl ($Rh^I(CO)_2$) species may be regarded as a result of the following reaction, involving OH groups of alumina when the support is not completely dehydroxylated [54]: $2Rh + 4CO + 2AlOH \rightarrow H_2 + 2Al\text{-}O\text{-}Rh^I(CO)_2$. This changes of dispersed Rh/Al_2O_3 catalysts by CO adsorption have also been observed in [55]. The intensity of the bands corresponding to νCO of geminal dicarbonyl species ($Rh^I(CO_2)$) decreases with the reduction temperature contrary to bands characteristics of monocarbonyl Rh(CO) species. The features of these spectra agree with those established earlier by Solymosi et al. [56]. Authors concluded that for the lower reduction temperature, CO adsorption leads to the disruption of the Rh clusters and to the formation of isolated Rh^I sites, as mentioned above. For higher temperature of reduction authors observed another effect, leading to the formation of Rh crystallites at the expense of Rh^I species.

In addition, it appears that supports with higher Lewis acidity are more likely to enhance the formation of Rh^I species [57,58]. As Ni incorporation influences directly the acidic properties of catalysts, an alteration on infrared spectra of adsorbed CO is expected. Indeed, infrared spectra of CO adsorbed on RhNi/Y-Al samples strongly differ from the others. In fact, the formation of CO complexes on oxidized rhodium particles ($Rh^I(CO_2)$) is strongly decreased in the presence of Ni, whatever the temperature. The geminal dicarbonyl species were still observed at reduction temperature of about 350 °C and 500 °C, but totally disappear at Tr = 650 °C. This feature is explained by the decrease of acidic properties of materials containing Ni, and therefore to a rearrangement of the hydroxyl groups of the catalyst. The presence of Ni at the support surface may also limit the Rh disruption.

4. Conclusion

The ethanol steam reforming reaction has been studied a lot for several years. However, it appeared recently that the use of a raw bioethanol feed is of a major importance to limit the purification steps and be effective for an industrial application. Nevertheless the presence of some impurities leads to an important deactivation of the catalysts during ESR. In order to enhance the catalyst stability for raw bioethanol steam reforming, we have studied here the effect of the addition of a second metal (Ni) on the catalytic behavior of a Y_2O_3-Al_2O_3 supported rhodium catalyst (Rh/Y-Al). The RhNi/Y-Al catalyst presented the highest hydrogen yield with the lowest amount of carbonaceous deposit. In a previous work, it was demonstrated that the catalytic performance of the Rh/Al_2O_3 base catalyst is improved by the doping with yttrium element and this is mainly due to the increase of the support basicity, the most basic support leading to the highest hydrogen yield and to the less stable coke. Acidity of the rare earth modified supports has also an important impact. In the present study, it is concluded that the addition of nickel to the Rh/Y-Al sample modify not only the metallic phase but also the support, with the formation of a $NiAl_2O_4$ phase at the support surface. Firstly, the basic properties fundamental for the high activity of catalysts in ethanol steam reforming are preserved and do not change with the emergence of the spinel $NiAl_2O_4$ structure. An important part of dispersed Ni still remains at the support surface. The presence of nickel reinforces the amount of weak LAS, thus preventing the catalyst deactivation by carbonaceous deposits. Secondly, the addition of nickel modifies the metallic phase by increasing the rhodium accessibility and stabilizing the rhodium particles, the presence of the nickel aluminate at the support surface allowing one to avoid the loss of rhodium by diffusion in the support bulk. At last, the presence of Ni^0 at the support surface may also be responsible for the higher hydrogen yield observed in the presence of the bimetallic catalyst compared to the monometallic Rh-Y-Al, which may be due to the activity of nickel for methane steam reforming and/or for ESR.

To conclude, in presence of methyl-2 propan-1-ol impurity, RhNi/Y-Al bimetallic catalysts present enhanced catalytic performances compared to the Rh/Y-Al monometallic catalyst, due to firstly, an optimum balance between support basicity and amount of strong Lewis acid sites, and secondly to an optimized metal function.

Acknowledgment

This work was supported by the French Environment and Energy Management Agency (ADEME) and the Poitou-Charentes Region.

References

[1] F. Auprêtre, C. Descorme, D. Duprez, Catal. Commun. 3 (2002) 263–267.
[2] F. Mariño, G. Baronetti, M. Jobbagy, M. Laborde, Appl. Catal. A 238 (2003) 41–54.
[3] F. Auprêtre, C. Descorme, D. Duprez, Top. Catal. 30 (2004) 487–491.
[4] A.N. Fatsikostas, X.E. Verykios, J. Catal. 225 (2004) 439–452.
[5] A. Birot, F. Epron, C. Descorme, D. Duprez, Appl. Catal. B 79 (2007) 17–25.
[6] A. Le Valant, A. Garron, N. Bion, F. Epron, D. Duprez, Catal. Today 138 (2008) 169–174.
[7] F. Auprêtre, C. Descorme, D. Duprez, D. Casanave, D. Uzio, J. Catal. 233 (2005) 464–477.
[8] A. Le Valant, Ph D Thesis, University of Poitiers 2008.
[9] A. Le Valant, F. Can, N. Bion, D. Duprez, F. Epron, Int. J. Hydrogen Energy (2009), doi:10.1016/j.ijhydene.2009.09.008.
[10] J.C. Vargas, S. Libs, A.-C. Roger, A. Kiennemann, Catal. Today 107–108 (2005) 417–425.
[11] S. Cavallaro, S. Freni, Int. J. Hydrogen Energy 21 (1996) 465.
[12] J. Comas, F. Mariño, M. Laborde, N. Amadeo, Chem. Eng. J. 98 (2004) 61–68.
[13] S. Cavallaro, V. Chiodo, S. Freni, N. Mondello, F. Frusteri, Appl. Catal. A 249 (2003) 119–128.
[14] W. Cai, F. Wang, A.C.V. Veen, H. Provendier, C. Mirodatos, W. Shen, Catal. Today 138 (2008) 152–156.
[15] N. Palmeri, S. Cavallaro, V. Chiodo, S. Freni, F. Frusteri, J.C.J. Bart, Int. J. Hydrogen Energy 32 (2007) 3335–3342.
[16] S. Natesakhawat, R.B. Watson, X. Wang, U.S. Ozkan, J. Catal. 234 (2005) 496–508.
[17] S. Natesakhawat, O. Oktar, U.S. Ozkan, J. Mol. Cat. A: Chem. 241 (2005) 133–146.
[18] B.S. Liu, C.T. Au, Appl. Catal., A 244 (2003) 181–195.
[19] F. Can, A. Le Valant, N. Bion, F. Epron, D. Duprez, J. Phys. Chem. C 112 (2008) 14145–14153.
[20] J. Kugai, V. Subramani, C. Song, M.H. Engelhard, Y.H. Chin, J. Catal. 238 (2006) 430–440.
[21] P.Y. Sheng, A. Yee, G.A. Bowmaker, H. Idriss, J. Catal. 208 (2002) 393–403.
[22] J.R. Rostrup-Nielsen, J. Catal. 31 (1973) 173–199.
[23] J.R. Rostrup-Nielsen, Catal. Today 18 (1993) 305–324.
[24] D.J. Pettigrew, D.L. Trimm, N.W. Cant, Catal. Lett. 28 (1994) 313–319.
[25] T. Bunluesin, R.J. Gorte, G.W. Graham, Appl. Catal. B 15 (1998) 107–114.

[26] Q. Fu, A. Weber, M. Flytzani-Stephanopoulos, Catal. Lett. 77 (2001) 87–95.
[27] S. Hilaire, X. Wang, T. Luo, R.J. Gorte, J. Wagner, Appl. Catal. A 215 (2001) 271–278.
[28] S. Colussi, C.d. Leitenburg, G. Dolcetti, A. Trovarelli, J. Alloys Compd. 374 (2004) 387–392.
[29] B. Harrison, A.F. Diwell, C. Hallett, Platinum Metals Rev. 32 (1988) 73–83.
[30] D. Duprez, M. Hadj-Aissa, J. Barbier, Appl. Catal. 49 (1989) 67–74.
[31] C. Li, T.C. Brown, Carbon 39 (2001) 725–732.
[32] C.-P. Hwang, C.-T. Yeh, Q. Zhu, Catal. Today 51 (1999) 93–101.
[33] D. Martin, D. Duprez, Appl. Catal., A 131 (1995) 297–307.
[34] J.C. Vis, H.F.J. van't Blik, T. Huizinga, J.V. Grondelle, R. Prins, J. Catal. 95 (1985) 333–345.
[35] W. Shan, M. Luo, P. Ying, W. Shen, C. Li, Appl. Catal., A 246 (2003) 1–9.
[36] G. Li, L. Hu, J.M. Hill, Appl. Catal. A 301 (2006) 16–24.
[37] M.E. Rivas, J.L.G. Fierro, R. Guil-Lopez, M.A. Pena, V.L. Parola, M.R. Goldwasser, Catal. Today 133 (2008) 367–373.
[38] Y. Cesteros, P. Salagre, F. Medina, J.E. Sueiras, Appl. Catal. B 25 (2000) 213–227.
[39] H.C. Yao, S. Japar, M. Shelef, J. Catal. 50 (1977) 407–418.
[40] J.E. Carpentier, J. Catal. 80 (1983) 472–478.
[41] M. Ferrandon, T. Krause, Appl. Catal. A 311 (2006) 135–145.
[42] H. Knözinger, P. Ratnasamy, Catal. Rev. - Sci. Eng. 17 (1978) 31–70.
[43] G. Busca, V. Lorenzelli, V.S. Escribano, R. Guidetti, J. Catal. 131 (1991) 167–177.
[44] F. Can, A. Travert, V. Ruaux, J.-P. Gilson, F. Maugé, R. Hu, R.F. Wormsbecher, J. Catal. 249 (2007) 79–92.
[45] E.P. Parry, J. Catal. 2 (1963) 371–379.
[46] S. Khabtou, T. Chevreau, J.-C. Lavalley, Microporous Mater 3 (1994) 133–148.
[47] C. Morterra, G. Magnacca, Catal. Today 27 (1996) 497–532.
[48] F. Abbattista, S. Delmastro, G. Gozzelino, D. Mazza, M. Vallino, G. Busca, V. Lorenzelli, G. Ramis, J. Catal. 117 (1989) 42–51.
[49] G.A.H. Mekhemer, Phys. Chem. Chem. Phys. 4 (2002) 5400–5405.
[50] G.A.M. Hussein, J. Phys. Chem. 98 (1994) 9657–9664.
[51] G. Busca, V. Lorenzelli, V.S. Escribano, Chem. Mater. 4 (1992) 595–605.
[52] C.A. Rice, S.D. Worley, C.W. Curtis, J.A. Guin, A.R. Tarrer, J. Chem. Phys. 74 (1981) 6487.
[53] J.B. Peri, J. Catal. 86 (1984) 84–94.
[54] H.F.J. Van't Blik, J.B.A.D. Van Zon, T. Huizinga, J.C. Vis, D.C. Koningsberger, R. Prins, J. Phys. Chem. 87 (1983) 2264–2267.
[55] D.J.C. Yates, L.L. Murrell, E.B. Prestridge, J. Catal. 57 (1979) 41.
[56] F. Solymosi, M. Pasztor, J. Phys. Chem. 89 (1985) 4789–4793.
[57] G. Lafaye, C. Mihut, C. Especel, P. Marécot, M.D. Amiridis, Langmuir 20 (2004) 10612–10616.
[58] S.D. Worley, C.A. Rice, G.A. Mattson, C.W. Curtla, J.A. Guln, A.R. Tarrer, J. Phys. Chem. 86 (1982) 2714–2717.